Journal of Computational Applied Mechanics 2021, 52(4): 553-569

DOI: 10.22059/jcamech.2021.326466.633

RESEARCH PAPER

# Contact mechanics of human knee joint: Analytical approach

Sachin Khot*, Ravi Guttal

*Center for Innovation and Product Development, KLE Technological University, Hubballi, 580031, India*

## Abstract

A new methodology for modeling tibio-femoral articular contact of a knee joint based on contact models of the classical contact mechanics is established. The given analytical models of articular contact are extended to the case of contact between low strain arbitrary linear elastic tissues, i.e., cartilages and meniscus. The approach uses the geometries of contact surfaces and the generalization of the Hertzian contact theory of non-conforming bodies with frictionless contact interaction between elastic articular tissues. The normal and tangential contact displacements are determined analytically based on the exact solutions for the spherical contact between the articular tissues of the knee. The non-linear stiffness (secant and tangential stiffness) of the knee joint's elastic half-space is derived using the analytical relationships. The method is demonstrated by exploring a case study, and the results are compared with the current literature to verify the fidelity of the proposed analytical approach. The analytical models facilitate accurate contact mechanics of the knee joint. Researchers may now use these analytical models to develop knee surrogate models in multibody dynamics.

**Keywords**: Knee joint slip, knee joint displacement, stick-slip zones, non-linear stiffness, geometric nonlinearities.

## 1. Introduction

Multibody dynamics (MBD) simulations of biological joints require modeling the internal forces inside the articular tissues [1]. In numerous MBD studies [2, 3, 4], the tibio-femoral articular contact is approximated as a rigid contact formulation, and single point contact takes place between the contacting bodies without any deformation. The deformable contacts must consider deformation behavior along with the articular surface geometry, and this is an added advantage is two-fold: 1) The deformable model provides better numerical stability during MBD; 2) It allows conforming surface geometries [5].

In the MBD of knee joints, efficient analytical models of deformable contact must be used to estimate contact parameters [6,7]. Several musculoskeletal models employ elastic foundation models to describe the deformable contact behavior of knee joints [5]. Lee et al. adopted the spline joints model to study the dynamics of the biological joints. The spline curves

* Corresponding author: sachin.khot@kletech.ac.in

and surfaces are primary elements in modeling the spline joints [8]. In other studies, Kok-Meng Lee et al. modeled two sequential circles rolling over a flat plane to mimic the functionality of the knee joint. The kinematics of this sliding contact is based on the trajectory of the multiple circles or lines, which resembles the knee functionality [9]. In these studies, the spline surfaces are deformed kinematically, and the surface itself did not participate in the dynamic simulation, and it fails to represent contact interaction under applied loads.

Finite-Element (FE) models have been extensively used to simulate the articular contacts of the knee joint over the last decade [10, 11]. The finite-element method can give full-field descriptions and handle complex geometrical configurations of articular contacts [12-13]. However, the FE preprocessing is excessively time-consuming in simulating the gait cycle. Novel-surrogate models have been exploited in recent years to simulate elastic contacts with a wide range of contact geometry[14, 15, 16]. This method is more computationally efficient and cost-effective than finite element contact models.

A new methodology for modeling tibio-femoral articular contact of a knee joint based on contact models of the classical contact mechanics is developed [17, 18, 19]. This approach uses the articular contact surface geometry and generalization of the Hertzian contact theory of non-conforming bodies with frictionless contact interaction between elastic articular tissues. The normal and tangential stiffnesses of the knee joint are determined analytically based on the exact solution for applied forces. According to [20], the anatomy-based MBD model necessitates precise data of the articular contact surfaces in solving the contact problem. Articular surfaces derived from experimental surface data are geometrically generalized in this approach. We are presenting the effective geometrical features of the articular surfaces for use in the joint contact mechanics of the knee joint, verifying the analytical solutions with the numerical and experimental case studies.

## 2. Material and methods

The material models are introduced in this part, including the mathematical strategy towards attaining analytical solutions.

### 2.1 Material properties of the Biological joints

The knee joint comprises deformable tissues such as cartilages, meniscus, and ligaments. Zielinska et al. have modeled the cartilage with isotropic elastic material models [21, 22]. Halonen et al. defined cartilage as a fibril-reinforced poro-viscoelastic material [23]. Wang et al. described the meniscus as a linearly elastic transversely isotropic material [24]. The linear elastic material models are used in this study to overcome the intricacies in arriving at mathematical models. Furthermore, this work does not address the study of material behavior.

Hard tissues are the bony members of the knee joint, including the Femur, Tibia, and Patella bones. Because the Femur and Tibia have little deformation compared to soft tissues, they are thought to be rigid bodies. [26, 27]. Bony tissues are considered rigid components in this study.

The knee joint is primarily the deformable contact made by cartilaginous tissue of the Femur and Menisci of the tibia. The $E_C$ and $\vartheta_C$ are the elastic modulus and Poisson's ratio of the cartilage. The $E_M$ and $\vartheta_M$ are the elastic modulus and Poisson's ratio of the menisci. The Boussinesq equation is being used to calculate the effective elastic modulus $E_{eff}$ at a given joint [28],

$$\frac{1}{E_{eff}} = \frac{1}{E^*} = \frac{1-\vartheta_C^2}{E_C} + \frac{1-\vartheta_M^2}{E_M} \tag{1}$$

**2.2 Mechanics of Biological joints**

There are two broad categories in contact mechanics based on the type of load acting on the joint: 1) normal load case; 2) combination of normal and tangential load case. This study does not investigate the tendons and ligaments that are active in tension but inactive in compressive loads. The synovial fluid film has a negligible influence because its thickness is quantified in micrometers. The applied normal force is shared among the lateral and medial condyles, and the moment about the femoral axis is accounted for. As the condyles are axisymmetric about their radius, hence the lever arm distances are $R_M$ and $R_L$. Thus the normal load taken by individual condyle can be calculated by following equations.

$$F_N = F_N^M + F_N^L \tag{2}$$

$$F_N^M = \frac{F_N \times R_M}{R_M + R_L} \tag{3}$$

$$F_N^L = \frac{F_N \times R_L}{R_M + R_L} \tag{4}$$

Here $F_N^M$ and $F_N^L$ - are the normal loads shared by the medial and lateral condyles, respectively. $R_M$ and $R_L$ - are the radius of curvatures of the medial and lateral condyles, respectively. The load acting on a given condyle is calculated by equations (3) and (4). The mathematical correlations have been established using the geometrical construction of the lateral condyle throughout this analytical procedure. The article's final section includes a case study on both the medial and lateral condyles.

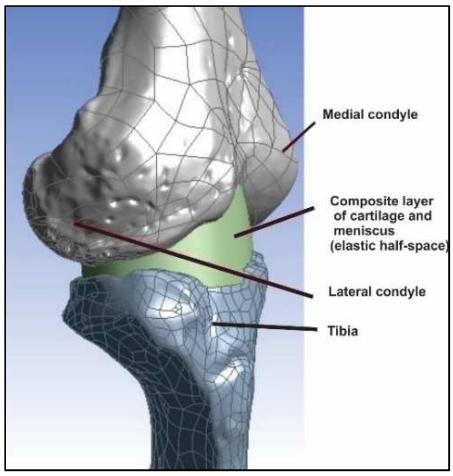


**Fig. 1** The CAD model of the knee joint

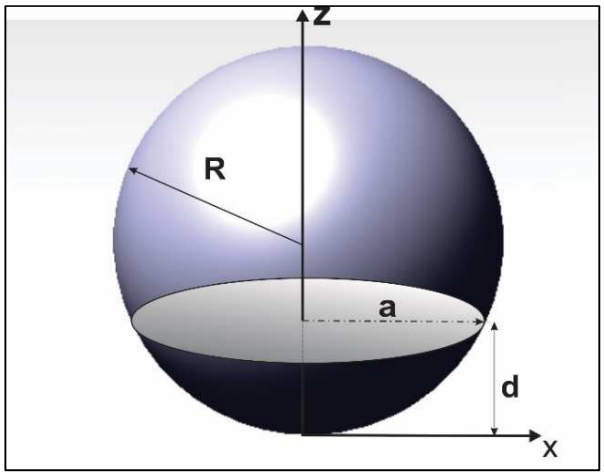


**Fig. 2.** Hertzian contact by Spherical condyle

The proportionality between incremental stiffness and the contact area is the fundamental property that permits dimensionality reduction to deformable contacts. Because this property exists among both normal and tangential contacts, it can be used to reduce the dimensionality of tangential contacts. The use of an elastic half-space method offers sophisticated solutions for smooth-edged and concentrated contacts [29]. The dimensionality reduction approach is utilized to change the 3-dimensional knee contact into a 2-dimensional contact; because the spherical knee condyle meets the axisymmetric requirement and can be reduced to a 2-dimensional problem.

### 2.3 Effect of Normal load on elastic Knee joints by Hertz Contact Problem

Deformable contact problems are addressed using Hertzian contact theory. This approach is used to investigate the joint's contact characteristics. The condyle resembles the shape of a sphere with a radius of curvature 'R', which is shown in Fig. 2. Let z and r be the normal and tangential directions with reference to the contact plane, respectively. The condyle acts as an indenter and develops the indentation profile. Fig. 4 is the geometrical construction of cartilage attached to condyle pressing the menisci under the action of normal and tangential loads.

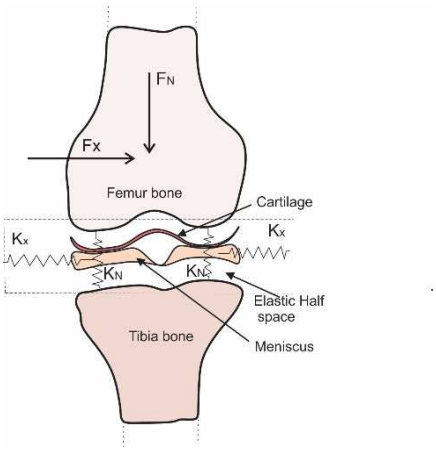


**Fig. 3** The system of normal ($F_z$) and tangential ($F_x$) loads on a knee joint

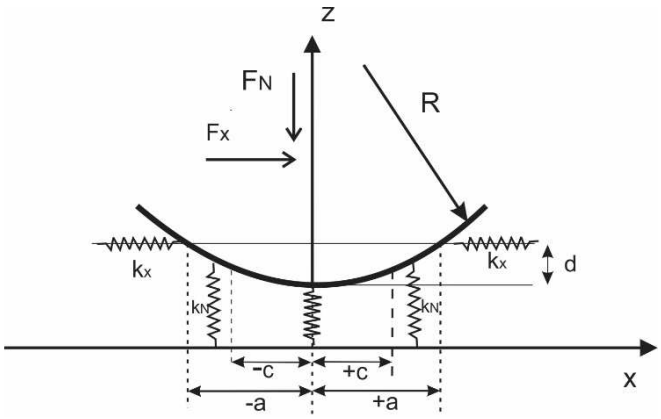


**Fig. 4** Geometrical constructions of contact under combined loads

Consider the effect of normal load ($F_N$) alone and assume the tangential load ($F_x$) is absent in Fig. 4. This is the 1-D analysis of a joint under normal loading. Let the elastic half-space be indicated by a single elastic spring, then according to Pythagorean Theorem,

$$(R - d)^2 + a^2 = R^2 \tag{5}$$

$$R - d = \sqrt{R^2 - a^2} \tag{6}$$

$$\frac{R - d}{R} = \sqrt{1 - \frac{a^2}{R^2}} \tag{7}$$

Applying the Binomial series expansion to simplify the Right-hand side of equation (7), then we get

$$1 - \frac{d}{R} \approx 1 - \frac{1}{2}\left(\frac{a^2}{R^2}\right) - O(\epsilon) \tag{8}$$

Since $\frac{a^2}{R^2} \ll 1$,

$$\frac{d}{R} \approx \frac{1}{2}\left(\frac{a^2}{R^2}\right) \tag{9}$$

$$d \approx \frac{a^2}{2R} \tag{10}$$

Therefore, the radius of contact, 'a' is given as,

$$\boldsymbol{a \approx \sqrt{2Rd}} \tag{11}$$

Let us consider that the cartilaginous condyle is pressed into the knee elastic half-space, shown in Fig. 4. The area of penetration has radius a. According to estimation rules, the dimensions of the heavily deformed area are on the same order of magnitude as the contact diameter 2a; hence the depth is ≈ 2a.

Approximating the elastic half-space as a cylinder of diameter 2a and depth 2a, the stiffness of the deformed body is

$$\mathrm{k} = \frac{\mathrm{E^*A}}{\mathrm{l}} = \frac{\mathrm{E^*}\,\pi\mathrm{a}^2}{2\mathrm{a}} \tag{12}$$

Now, the force applied on an elastic body in terms of stiffness can be written as follows,

$$F = k \times d = \frac{E^*\,\pi a^2}{2a} \times d \tag{13}$$

$$F = \frac{E^*\,\pi\,\left[\sqrt{2Rd}\right]}{2} \times d \tag{14}$$

$$F = \frac{\pi E^*}{2}\; d^{3/2}\,\left[\sqrt{2R}\right] \tag{15}$$

$$\boldsymbol{d} = \left[\frac{\mathbf{2}}{\boldsymbol{\pi^2\,R}}\left(\frac{\boldsymbol{F}}{\boldsymbol{E^*}}\right)^{\mathbf{2}}\right]^{1/3} \tag{16}$$

Equation (16) is used to estimate the depth of penetration of the condyle into the elastic half-space under the normal loading.

### 2.4 The combined effect of normal and tangential load on a knee joint

The tangential loading is prominently seen during the gait cycle and where the knee is under a complex system of loads. The normal load is acting on the knee joint, which presses the condyle into the elastic cartilaginous tissue and menisci. Subsequently, a small amount of tangential force is applied to the condyle, which results in a transverse displacement. The frictional forces govern this with the coefficient of friction (μ) and transverse shear forces. The inner zone of this spherical contact is known as the stick zone. If tangential force is slightly increased, that results in shrinkage of the stick zone and an increase in the slip zone. The tangential stresses tend to be maximum at the stick boundary, minimum at the mid-point of the contact, and zero at the contact boundary (a). The normal stresses are maximum at the mid-point of the joint and zero towards the boundary. The stick and slip zones are shown in Fig. 5.

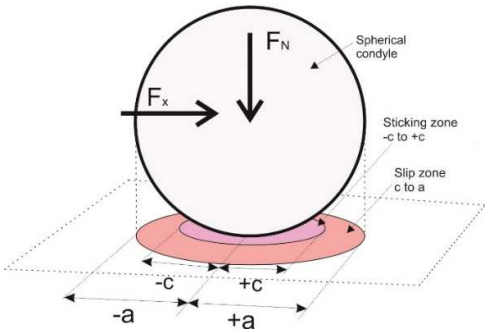


**Fig. 5** The concept of the stick and non-stick zones

This section analyzes the combined effect of normal and tangential forces Tangential load results in the relative transverse displacement between the mating surfaces along the x-direction. Consider Fig. 4, in which the geometrical construction of the knee joint under the combined loading conditions is shown. The normal displacement and the transverse displacement of the joint because of the normal load $F_N$ and tangential load $F_x$ are derived in subsequent paragraphs.

We consider the spherical condyle surface of radius R, which has penetrated the linear elastic foundation by depth d, as shown in Fig. 4. Here the knee joint space with the cartilage of the Femur is pressed into the menisci of the knee joint by the normal force $F_N$ and subsequently, the joint is loaded by a horizontal tangential force $F_x$. The coefficient of friction μ exists between the two elastic contact bodies due to adhesive action under the tangential load $F_x$. Based on geometrical formulation, the displacement of elastic spring media along z-direction at any radial distance 'x' from the midpoint of contact is given by [30],

$$\boldsymbol{u_z(x) = d - \frac{x^2}{2R}} \tag{17}$$

The elastic force at a distance x across the contact radius can be written as follows,

$$F_N(x) = stiffness \times displacement = (E^* \frac{l}{l} \Delta x).u_z(x)$$

$$= \left(d - \frac{x^2}{2R}\right) E^* \ \Delta x \tag{18}$$

The tangential stiffness $\Delta k_x$ of the stick zone in the given biological joint is provided by,

$$\boldsymbol{\Delta k_x = G^* \Delta x} \qquad x \in [\,0, c\,] \tag{19}$$

Where, $G^*$ is known as an effective shear modulus of mating bodies, and it is given by [20],

$$\frac{1}{G^*} = \frac{2-\vartheta_c}{4G_c} + \frac{2-\vartheta_M}{4G_M} \tag{20}$$

- $G_C$ & $\vartheta_C$ = Shear moduli and Poisson's ratio of the cartilage tissue,
- $G_M$ & $\vartheta_M$ = Shear moduli and Poisson's ratio of the menisci tissue,

If $u_x$ is the transverse displacement of the body along the x-direction, then $F_x(x)$ is the tangential force acting across the slip zone, which is between 0 to c and is given by,

$$F_X(x) = \Delta k_x \ u_x = (G^* \Delta x) \ u_x \qquad for, \boldsymbol{0 < x \leq c} \tag{21}$$

We have x = ± c, which is the boundary of the stick zone, where the tangential force is equal to the frictional force, that is

$$F_X(c) = \mu\, F_N(c) \tag{22}$$

Where c is the contact boundary of the stick zone, then the equation (22) is valid at x = c, and beyond that area, the slip zone exists. Now, substitute Equation (18) and (21) in (22), then

$$G^* \Delta x \ u_x = \mu \left(d - \frac{x^2}{2R}\right) E^* \ \Delta x \tag{23}$$

$$\boldsymbol{u_x = \mu \frac{E^*}{G^*}\left[d - \frac{c^2}{2R}\right] = constant \qquad for \quad 0 < x \leq c} \tag{24}$$

Hence equation (24) gives the amount of transverse shear displacement along the x-direction in the stick zone of the contact. If the entire area of contact between the radial boundaries –a to a is considered along the x-direction, then the normal force acting on the given biological joint can be given as [21],

$$F_N = \int_{-a}^{a} \left[d - \frac{x^2}{2R}\right] E^* dx \tag{25}$$

$$F_N = E^* \int_{-a}^{a} \left[\frac{a^2}{2R} - \frac{x^2}{2R}\right] dx \tag{26}$$

$$F_N = \frac{E^*}{2R}\left[2a^3 - \frac{2}{3}a^3\right] \tag{27}$$

$$\boldsymbol{a} = \left[\frac{\mathbf{3}\,\boldsymbol{R}\,\boldsymbol{F_N}}{\mathbf{2}\,\boldsymbol{E^*}}\right]^{1/3} \tag{28}$$

The equation (28) can be used to estimate the contact radius 'a' of the knee condyle during the normal loading. The maximum depth of penetration because of the applied normal force is given by,

$$\boldsymbol{d} = \frac{\mathbf{1}}{\mathbf{2}\boldsymbol{R}^{1/3}} \left[\frac{\mathbf{3}\,\boldsymbol{F_N}}{\mathbf{2}\,\boldsymbol{E^*}}\right]^{2/3}$$

$$= \mathbf{0.6551} \left[\frac{\boldsymbol{F_N}}{\boldsymbol{E^*}}\right]^{2/3} \frac{\mathbf{1}}{\boldsymbol{R}^{1/3}} \tag{29}$$

The total tangential force is estimated as the sum of the transverse shear force and the tangential frictional force induced in the given biological joint, which can be calculated as follows [21-22],

$$F_x = 2\int_0^c [G^*\ u_x\ dx\ ] + 2\mu \int_c^a \left[d - \frac{x^2}{2R}\right] E^* dx \tag{30}$$

$$F_x = 2\int_0^c \left[G^*\ \mu\ \frac{E^*}{G^*}\left[d - \frac{c^2}{2R}\right]\ dx\ \right] + 2\mu \int_c^a \left[d - \frac{x^2}{2R}\right] E^* dx \tag{31}$$

$$F_x = 2\mu\int_0^c \left[E^*\ \left[\frac{a^2}{2R} - \frac{c^2}{2R}\right]\ dx\ \right] + 2\mu \int_c^a \left[\frac{a^2}{2R} - \frac{x^2}{2R}\right] E^* dx \tag{32}$$

$$F_x = 2\mu E^* \left[\frac{ca^2}{2R} - \frac{c^3}{2R} + \frac{c^3}{6R} - \frac{ca^2}{2R} + \frac{a^3}{3R}\right] \tag{33}$$

$$F_x = \frac{2\mu E^* a^3}{3R}\left[1 - \frac{c^3}{a^3}\right] = \mu\, F_N \left(1 - \left(\frac{c}{a}\right)^3\right) \tag{34}$$

$$\boldsymbol{c} = \boldsymbol{a}\left[\mathbf{1} - \frac{\mathbf{3}\boldsymbol{R}}{\mathbf{2}\mu\boldsymbol{a^3}}\frac{\boldsymbol{F_x}}{\boldsymbol{E^*}}\right]^{1/3} = \boldsymbol{a}\left[\mathbf{1} - \mu\frac{\boldsymbol{F_x}}{\boldsymbol{F_N}}\right]^{1/3} \tag{35}$$

Equation (35) estimates the radius of the stick zone in a combined load ($F_x$ and $F_N$) & knee joint. The tangential load and normal load contribute to calculating the contact radius (c). The radius (c) of the stick area always controls the slip or tangential displacement $u_x$ in the given joint. The slip is said to be maximum when the stick zone is absent. Thus when c = 0, from equation (24)

$$\boldsymbol{u_{x,max}} = \boldsymbol{\mu}\,\frac{\boldsymbol{E^*}}{\boldsymbol{G^*}}\boldsymbol{d} \tag{36}$$

Hence the equation (36) gives the value of maximum slip that is possible in a given biological joint when there is no stick zone, and it is dependent on the depth of penetration d. Also, when c=0, the relationship between the $F_x$ and $F_N$ can be found by equation (34),

$$F_x = \mu F_N \left(1 - \left(\frac{0}{a}\right)^3\right) \tag{37}$$

$$\boldsymbol{F_x} = \mu \boldsymbol{F_N} \tag{38}$$

The total transverse displacement in x-direction could be given by the sum of shear displacement in the stick zone and the frictional displacement in the slip area between the radii c to a [10].

$$u_x^{Total} = u_x^c + u_x^{c,a} = \mu \frac{E^*}{G^*}\left[d - \frac{c^2}{2R}\right] + \mu\left[d - \frac{x^2}{2R}\right] \tag{39}$$

The shear displacement $u_x^c$ is constant in $|0 < x \leq c|$ and the frictional displacement $u_x^{c,a}$ is valid in $|c < x \leq a|$. We can use the Heaviside function H(x) to write the $u_x^{Total}$.

$$u_x^{Total} = \mu \frac{E^*}{G^*}\left[d - \frac{c^2}{2R}\right] + H(x)\,\mu\left[d - \frac{x^2}{2R}\right] \tag{40}$$

Where $H(x) = \begin{cases} 0, & when \quad 0 < x \leq c \\ 1, & when \quad c < x < a \end{cases}$

### 2.5 Stiffness of the soft tissues in knee joint

The ratio of applied force to the corresponding displacement of an elastic body results in material stiffness 'k'. The experimental data are collected from previous studies on biological joints. Firstly, consider the normal force and displacement relation, which is derived from 1-D analysis, which is given in equation (16), then the normal secant stiffness (Average stiffness) can be given by equation (41) and is shown in Fig. 7.

$$\frac{F}{d} = 2.221\, E^*\, R^{1/2}\, d^{1/2} \tag{41}$$

The tangential stiffness (Instantaneous stiffness) is given by the derivative of force w.r.t displacement given by equation (42)

$$\frac{\partial F}{\partial d} = 3.333\, R^{1/2}\, d^{1/2} \tag{42}$$

Equations (41) and (42) give the non-linear stiffness relation when we consider the 1-D analysis of a given joint using a single spring model.

The normal force that is calculated by considering 2-D analysis by variation in radius of contact across the x-direction, which is given in equation (29), is used to calculate the normal secant stiffness (Average stiffness) and is shown in Fig. 8.

$$\frac{F}{d} = 1.885\, E^*\, d^{1/2}\, R^{1/2} \tag{43}$$

The tangential stiffness (Instantaneous stiffness) is given by the derivative of force w.r.t displacement given by equation (44)

$$\frac{\partial F}{\partial d} = 2.827\, R^{1/2}\, d^{1/2} \tag{44}$$

The equations (41) and (44) indicate the non-linear nature of joint stiffness under normal loading. This is a feasible method of calculating the stiffness of a given biological joint.

## 3. Case Studies on Biological Joints

This section includes the results of case studies determined using two case studies by different methods. Firstly, knee joint contact mechanics are analyzed using the analytical

models derived in previous sections of this article. Secondly, the knee joint contact mechanics is analyzed using the numerical method (FE analysis).

### 3.1 Materials

A man who weighs 70 Kg is standing on one foot. The tibia and femur axis are assumed to be colinear and vertical. The radius of curvature of the medial condyle and lateral condyle is 21mm and 24mm, respectively. The data is collected from experimental biomechanics. Given Young's modulus, shear modulus, and Poisson's ratio of articular cartilage are 12MPa, 4.02MPa, and 0.49, respectively. The Young's modulus, shear modulus, and Poisson's ratio of Menisci are 59MPa, 19.79MPa, and 0.49. The coefficient of friction between the articular surfaces is 0.3. The transverse load of 10Kg is acting on Femur through the posterior plane [31, 32]. Referring to the numerical case study, the EHS is defined as an isotropic elastic material with Young's modulus of 13.12 MPa, a Poisson's ratio of 0.3, and a density of 1000 $kg/m^3$ [5-7].

In this case, the values of $F_N = 686.9N, F_x = 98.1N, E_M = 59MPa, E_L = 12MPa, G_M = 19.79MPa, G_L = 4.02\ MPa, R_M = 21mm, R_L = 24mm$ and $\mu = 0.3$ are known and collected from biomechanics studies [31, 32]. From equation (1), the effective elastic modulus is found to $E^*$=13.12Mpa.

### 3.2 Methods

#### 3.2.1 Analytical Method

The first method is a one-dimensional analysis of the knee joint. The second method evaluates the knee joint under 2-dimensional loading as described in earlier sections. The radius of the condyle's curvature is utilized to quantify the load carried by each condyle separately. Firstly, the depth of penetration(d) is calculated by using equation (29). The radius of contact (a) is calculated by using equation (28). The radius of the stick boundary (c) is found given by equation (35). The maximum tangential displacement ($u_x$ ) is estimated through equations (40).

#### 3.2.2 Numerical method (Finite element analysis)

The spherical lateral condyle is pressing over the cylindrical surface of elastic cartilage and meniscus tissues. The purpose of developing this Tibio-Femoral (TF) model was to estimate the stiffness behavior of the knee joint. The 3D CAD models of the sphere and cylindrical EHS are developed by the 3D experience CAD tool (Dassault systems, SE). The condyle of the femur bone is modeled as a rigid sphere, and the soft tissues of Elastic-Half Space (EHS) are described as a deformable component. The Hexahedral C3D8R: 8-node linear brick, reduced integration, hourglass control mesh is generated on the cylindrical EHS geometries in ABAQUS tool (ABAQUS Inc., Providence, RI) through medial axis algorithm. The reduced integration element is chosen to prevent volumetric locking in the numerical model. The rigid discrete R3D4: 4-node 3-D bilinear rigid quadrilateral mesh is used to mesh the rigid sphere. The global sizing tool is set to an average 1 mm mesh element size for the EHS [36, 37, 38].

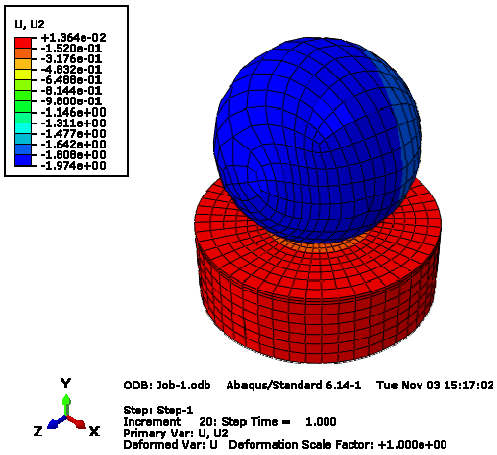


**Fig. 11** Three Dimensional FE Model

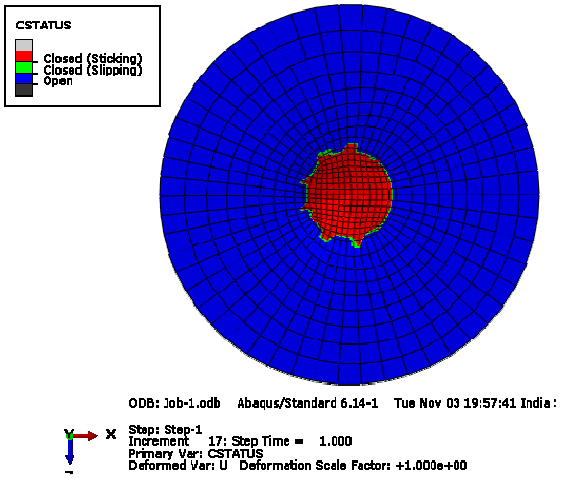


**Fig. 12** Contact regions: Sticking and Slipping zones

**Contact definitions.** The contact model was created in ABAQUS, as shown in Fig. 11. A surface-to-surface standard contact model with the finite sliding formulation is used to provide a computationally efficient characterization. The contact interaction has the tangential behavior with penalty friction formulation with a coefficient of friction 0.15 is developed. The outer surface of the rigid sphere is defined as a master surface, and the deformable EHS surface is defined as a slave surface.

**Boundary and loading conditions.** The bottom surface of a deformable EHS body is fixed by constraining all the degrees of freedom. The linear perturbation step is used to apply the two loads steps. During the first step, a 1µm of displacement in the y-direction is applied on a rigid sphere; then, in the second step, a normal downward force of -354.8N is applied to the reference point provided on the rigid sphere. In this study, numerical solutions are only restricted to normal loading cases [38, 39].

**Mesh convergence.** After defining material modeling, boundary conditions, and loading conditions, sensitivity analyses on mesh density were performed. The element size of the EHS component was varied to yield six different mesh resolutions by keeping the very refined mesh as the reference for comparison (Table 2). The peak directional displacements predicted by cases a-e were compared with those predicted by the reference case, and the cases within ±5% of the reference case were considered as accurate. Case c was optimal, as it requires less computing power while maintaining a prediction accuracy of 96% concerning the reference case model. The sensitivity study resulted in 5608 numbers of C3D8R elements (1mm size) for the EHS.

**Table 2.** Sensitivity analyses on mesh density for different knee substructures.

| Case(s) | Reference | Case a | Case b | Case c | Case d | Case e |
|---|---|---|---|---|---|---|
| **Element Size in (mm)** | 0.3 | 0.5 | 0.75 | 1 | 1.25 | 2 |
| **Number of Elements** | 16567 | 12761 | 7632 | **5608** | 3708 | 2342 |
| **% Change in Peak Directional Displacements** | -- | 1.73 | 2.86 | **3.45** | 8.05 | 14.35 |

## 4. Results and Discussion

**Discussion on Analytical solutions.** The solutions are evaluated from the case studies through using analytical models established for 1D and 2D analysis, as shown by Table.1.

**Table. 1** Analytical solutions of case study

| **According to 2-D analysis** | | | | |
|---|---|---|---|---|
| | **Medial Condyle** | | **Lateral Condyle** | |
| Radius of curvature | $R_M$ | 21mm | $R_L$ | 24mm |
| Normal force | $F_N^M$ | 331.8N | $F_N^L$ | 354.8N |
| Tangential force | $F_x^M$ | 47.4N | $F_x^L$ | 50.68N |
| Displacement | d | 2.047mm | d | 2.048mm |
| Radius of contact | a | 9.27mm | a | 9.91mm |
| The radius of the stick boundary | c | 7.47mm | c | 7.99mm |
| Maximum tangential displacement | $u_x$ | 0.29mm | $u_x$ | 0.31mm |
| **According to 1-D analysis** | | | | |
| Displacement | d | 1.834mm | d | 1.834mm |

Fig. 6 is used to relate the normal displacement ($\mathbf{u_z}$) and corresponding contact radius along the x-direction. At the mid-point of the contact where x=0, the normal displacement $\mathbf{u_z}$ is maximum. But, towards the contact boundary, the $\mathbf{u_z}$ approaches to zero.

The normal displacement ($\mathbf{u_z}$) and associated contact radius along the x-axis are shown in Fig. 6. The normal displacement $\mathbf{u_z}$ is maximum at the contact's midpoint (at x=0). Consequently, as the contact boundary approaches, the $\mathbf{u_z}$ approaches zero.

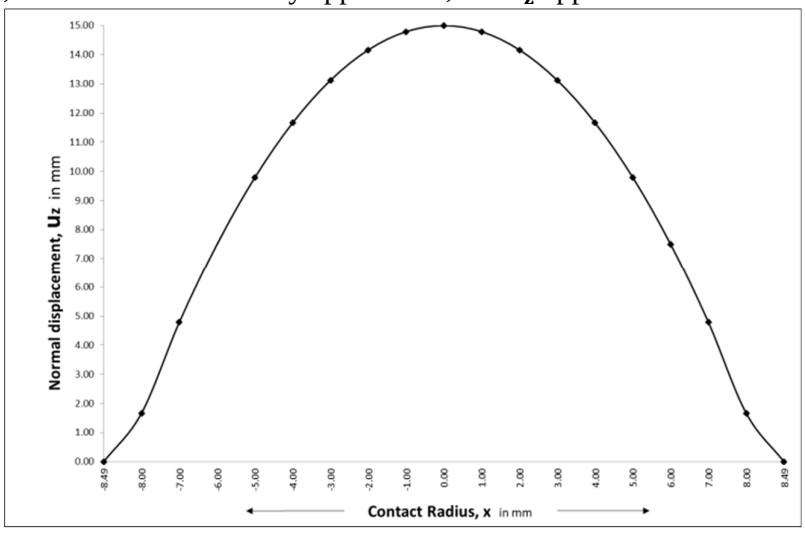


**Fig. 6** Variation of $u_z$ with Contact Radius x

This stiffness can be estimated by calculating the slope of the trend line F versus d, which is shown in Fig. 7.

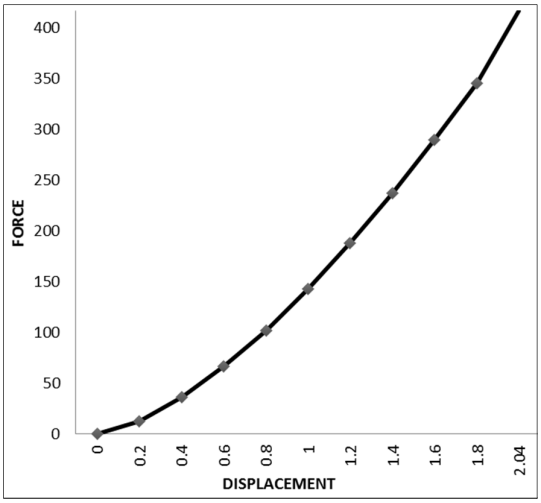


**Fig. 7** Normal Force vs. displacement in 1-D analysis

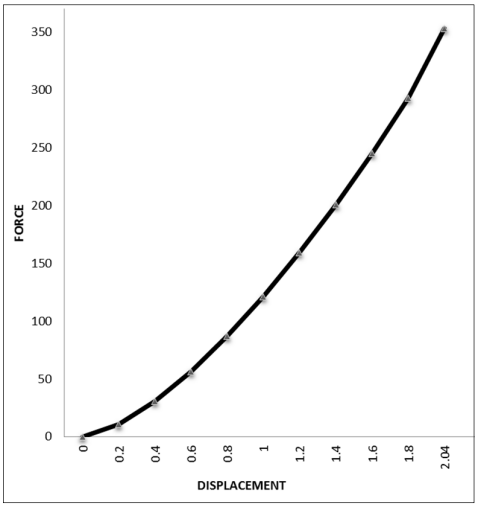


**Fig. 8** Normal Force vs. displacement in 2-D analysis

Fig. 9 gives the curve of total tangential displacement versus the contact radius in the medial condyle. The tangential shear displacement within the stick zone is $u_x^c = 0.142\text{mm}$ and is constant up to c=7.47mm because the sticking action is not permitting any relative slip. The slip in the non-stick zone between[c, a] is $u_x^{c,a}$ and at this zone, the maximum transverse displacement in the joint surface is seen.

Fig. 10 gives the curve of total tangential displacement versus the contact radius in lateral condyle. The tangential shear displacement within the sticking zone is $u_x^c = 0.1042\text{mm}$ and constant up to c = 7.9905mm. In this analytical approach, various aspects of biological joints, such as the material properties, contact geometry, and deformation mechanism, are explored.

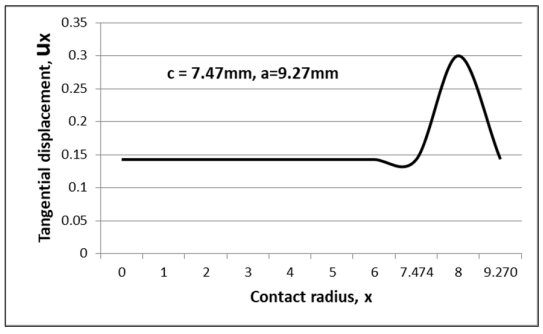


**Fig. 9** Tangential displacement versus contact radius in the medial condyle

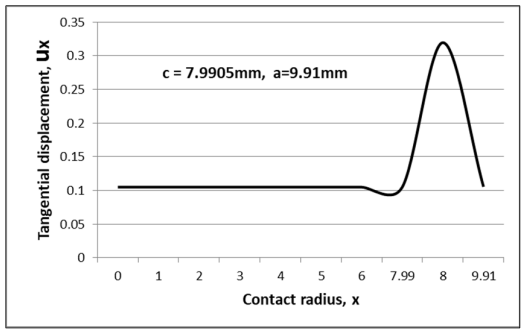


**Fig. 10** Tangential displacement versus contact radius in the lateral condyle

**Discussion on numerical (FE) solutions.** The deformed contour plots are shown in Fig. 11. The contours of the contact zone are shown in Fig. 12. The red zone indicates the stick zone of the contact, where there is no tangential deformation/slip seen. The small ring of the green area indicates the portion of the slip zone present in the given contact surface. In this analysis, the tangential slip is 0.216mm along the direction of tangential loading (x-direction).

A similar explanation of the analytical method can be adopted to describe the contact interactions in numerical analysis. The force versus displacement plots is post-processed, as shown in Fig. 13. The numerical solutions are found to be in close agreement with experimental and analytical solutions. The comparison of normal displacements in the numerical, analytical, and clinical methods is given in Table 3. The analytical solution is found to agree with numerical and experimental solutions.

**Comparative discussion on results of the analytical, numerical, and experimental methods.** The primary goal of this work was to estimate the stiffness behavior of the biological joints. In this section, the relative behavior of force and corresponding displacement is given on a single plot. The one-dimensional spring approach is used to characterize the effect of geometrical nonlinearity on joint stiffness. The solid lined curve in the plot given by Fig. 13 can be used to assess the non-linear stiffness in the case of one-dimensional analysis. The 2 D analytical formulations derived in this study are used to estimate the stiffness plots, which are shown by the dash lined curve with diamond markers.

**Table. 3** Comparision of solutions of the case study

| **Lateral condyle** | | | **Directional displacement in** | | |
|---|---|---|---|---|---|
| | | | Numerical method(FE) | Analytical Method | Experimental/clinical Method [27-28] |
| Radius of curvature | $R_L$ | 24mm | 1.837mm | 2.048mm | 1.54mm |
| Max. Normal force | $F_N^L$ | 354.8N | | | |
| Elastic modulus | E | 13.12N/mm$^2$ | | | |

The finite element method is used to assess the knee joint stiffness, which considers the geometrical nonlinearities. The stiffness behavior of the knee joint contact models is said to be similar in all cases. As stiffness is a fundamental property of any biomechanical system, and that can be used in co-simulation studies. Thus, any living joint's behavior depends on the geometrical parameters of the contact and the material behavior of constitutive tissues.

The finite element method, which takes into account geometrical nonlinearities, is being used to quantify knee joint stiffness. In all scenarios, the stiffness characteristic of the knee joint contact models is reported the same. As stiffness is a fundamental property of any biomechanical system, and in a nutshell, the functionality of every physiological joint is influenced by the contact's geometrical parameters, including the constituent tissue's material behavior.

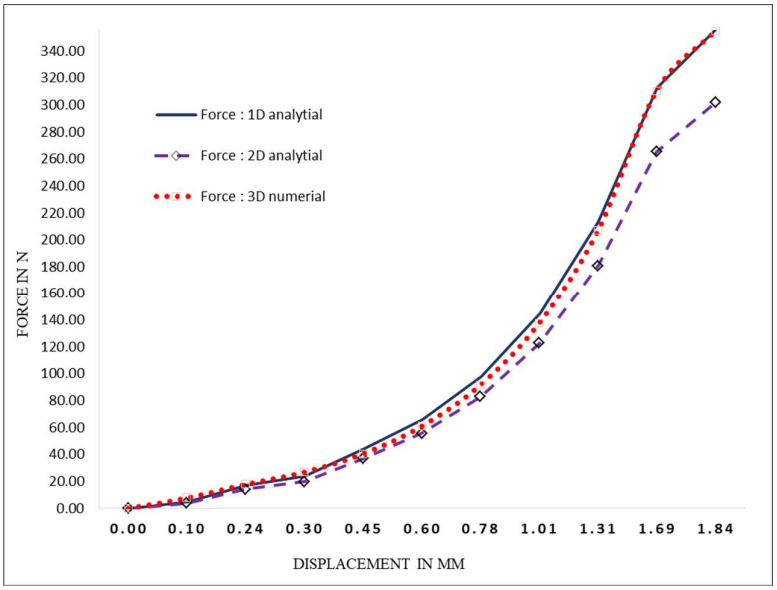


**Fig. 13** Comparision of joint stiffness behavior of analytical and numerical methods

Biological joints play a significant role in the movements and activities of living animals. Two different scenarios are extensively investigated in this work. The first scenario involves normal forces acting on contact surfaces, for which a mathematical formulation is established. The Boussinesq equations are implemented appropriately to evaluate the effective elastic modulus of the two mating bodies in a given joint. The normal displacement or deformation caused by normal loading in the joint is evaluated explicitly. The second step is to model the deformation of the knee joint as a function of combined loading. The contact area radius (a) and the stick boundary radius (c) are also established. Finally, a case study has been included to provide a more precise implementation of the current studies.

Though validation of this analytical methodology is beyond the scope of this paper, correlations between experimental data and numerical solutions revealed that the current approach generates credible predictions. Experimental observations were compared to the contact displacements estimated by the knee contact model [40, 41]. The non-linear contact response was predicted using linear material parameters. The analytical model can accurately estimate normal displacement, tangential displacement, contact forces, and the widths of the contact areas (Slip and stick zones) for a ramped load of 708 N. These findings are crucial in assessing the capabilities and limitations of the current contact models and can be improved as new understanding is gained.

## 5. Conclusions

The long-term goal is to incorporate deformable contact models of knee joints into multibody dynamic musculoskeletal models created with programs such as OpenSim or ADAMS. In summary, this paper has presented a detailed methodology for incorporating a deformable contact knee model for static analysis. The current implementation works for the tibiofemoral joint of natural knees and can accommodate small and large strain contact models with linear material properties. The methodology can predict normal displacement, tangential displacement, contact forces, and sizes of the contact areas (Slip and stick zones) and is computationally fast to perform static simulations of the tibiofemoral joint.

The analytical model can be used as a surrogate joint model in dynamic analysis of the body with multiple joints. The future scope of the study directs to the development of

mathematical models by utilizing the contact mechanics formulations to study the dynamic behavior of animal joints. This analytical approach can be further explored for other biological joints. The unique use of the current work is made in co-simulation models for kinematic analysis of knee joints, where the joint stiffness is derived from this analytical formulation. The analytical model can be used to solve an inverse problem. In the future, the non-linear characteristics of the biological joints are to be compared with the numerical techniques. The stiffness formulations shall be used as surrogate joint characteristics in dynamic joint analysis using multibody dynamics and co-simulation. We have found several potential computational and functional enhancements areas using analytical solutions. The addition of patellofemoral contact using the patella would enhance the current model's utility. The limitations of this method are that the full-field descriptions cannot be determined using these models and are given as a lumped parameter system.

**Acknowledgments**

The author acknowledges that this work has been supported by the Center for Innovation and Product Development (http://cipd.kletech.ac.in), School of Mechanical Engineering, KLE Technological University, Hubballi.

**Conflict of interest statement**

The authors declare that they have no conflict of interest.

**References**

1. W. Herzog and S. Federico, Considerations on Joint and Articular Cartilage Mechanics. Biomechanics and Modeling in Mechanobiology, 5, 64–81, 2006.
2. J. Wismans, F. Veldpaus, J. Janssen, A. Huson, and P. Struben, A Three-Dimensional Mathematical Model of the Knee-Joint, Journal of Biomechanics, 13, 677–679, 681–685,1980.
3. E.M. Abdel-Rahman and M.S. Hefzy, Three-Dimensional Dynamic Behaviour of the Human Knee Joint Under Impact Loading, Medical Engineering & Physics, 20, 276–290, 1998.
4. Z.-K. Ling, H.-Q. Guo, and S. Boersma, Analytical Study on the Kinematic and Dynamic Behaviors of a Knee Joint, Medical Engineering & Physics, 19, 29–36, 1997.
5. L. Blankevoort, J.H. Kuiper, R. Huiskes, and H.J. Grootenboer, Articular Contact in a Three-Dimensional Model of the Knee, Journal of Biomechanics, 24, 1019–1031, 1991.
6. Y. Bei and B.J. Fregly, Multibody Dynamic Simulation of Knee Contact Mechanics. Medical Engineering & Physics, 26, 777–789, 2004.
7. M. Machado, P. Flores, J.C.P. Claro, J. Ambrosio, M. Silva, A. Completo, and H.M. Lankarani, Development of a Planar Multibody Model of the Human Knee Joint, Nonlinear Dynamics, 60, 459–478, 2010.
8. Lee, S. H., & Terzopoulos, D. (2008). Spline joints for multibody dynamics. ACM Transactions on Graphics, 27(3). https://doi.org/10.1145/1360612.1360621
9. Lee, K. M., & Guo, J. (2010). Kinematic and dynamic analysis of an anatomically based knee joint. Journal of Biomechanics, 43(7), 1231–1236. https://doi.org/10.1016/j.jbiomech.2010.02.001
10. W. Wilson, C. C. van Donkelaar, R. van Rietberger, and R. Huiskes, The Role of Computational Models in the Search for the Mechanical Behaviour and Damage

Mechanisms of Articular Cartilage, Medical Engineering and Physics 27, 810–826, 2005.
11. J. Z. Wu, W. Herzog, and M. Epstein, Evaluation of the Finite Element Software ABAQUS for Biomechanical Modelling of Biphasic Tissues, Journal of Biomechanics, 31, 165–169, 1997.
12. DI. Caruntu and M.S. Hefzy, 3-D Anatomically Based Dynamic Modeling of the Human Knee to Include Tibio-Femoral and Patello-Femoral joints, Journal of Biomechanical Engineering, 126, 44–53, 2004.
13. A. P´erez-Gonzalez, C. Fenollosa-Esteve, J.L. Sancho-Bru, F.T. Sanchez-Marin, M. Vergara, and P.J. Rodriguez-Cervantes, A Modified Elastic Foundation Contact Model for Application in 3D Models of the Prosthetic Knee, Medical Engineering & Physics, 30, 387–398, 2008.
14. Y.-Ch. Lin, R.T. Haftka, N.V. Queipo, and B.J. Fregly, Surrogate Articular Contact Models for Computationally Efficient Multibody Dynamic Simulations, Medical Engineering & Physics, 32, 584–594, 2010.
15. Ilan, Eskinazi., & Benjamin, J, Fregly. (2016). An open-source toolbox for surrogate modeling of joint contact mechanics. IEEE transactions on biomedical engineering, vol.63, No. 2.
16. Roman, Pryazhevskiy., Ildar, Akhtyamov., Anna, Morgunova., Helo, Mohammad, Jihad., & Andrey, Nevzorov. (2020). Springer Nature Switzerland AG 2020, IHIET, AISC 1018, pp.612-617.
17. Popov, V. L., Heß, M., Willert, E., Popov, V. L., Heß, M., & Willert, E. (2019). Normal Contact Without Adhesion. In Handbook of Contact Mechanics. https://doi.org/10.1007/978-3-662-58709-6_2
18. Lee, E. H. (1955). Stress analysis in visco-elastic bodies. Quarterly of Applied Mathematics, 13(2), 183–190. https://doi.org/10.1090/qam/69741.
19. LD Landau, E.M. Lifschitz, Theory of elasticity (Theoretical Physics, Vol7), 3rd edition, 1999, Butterworth-Heinemann, Oxford, 8,9.
20. DI. Caruntu and M.S. Hefzy, 3-D Anatomically Based Dynamic Modeling of the Human Knee to Include Tibio-Femoral and Patello-Femoral joints, Journal of Biomechanical Engineering, 126, 44–53, 2004.
21. Zielinska, B., & Donahue, T. L. H. (2006). 3D finite element model of meniscectomy: Changes in joint contact behavior. Journal of Biomechanical Engineering, 128(1), 115–123.
22. Anderson, A. E., et al. (2005). Subject-specific finite element model of the pelvis: development, validation and sensitivity studies. Journal of Biomechanical Engineering, 127(3), 364–373.
23. Halonen, K. S., et al. (2014). Deformation of articular cartilage during static loading of a knee joint–experimental and finite element analysis. Journal of Biomechanics, 47(10), 2467–2474.
24. Wang, Y., Fan, Y., & Zhang, M. (2014). Comparison of stress on knee cartilage during kneeling and standing using finite element models. Medical Engineering & Physics, 36(4), 439–447.
25. Adouni, M., Shirazi-Adl, A., & Shirazi, R. (2012). Computational biodynamics of human knee joint in gait: from muscle forces to cartilage stresses. Journal of Biomechanics, 45(12), 2149– 2156.
26. Adams, C. R., et al. (2007). Effects of rotator cuff tears on muscle moment arms: A computational study. Journal of Biomechanics, 40(15), 3373–3380.

27. Zheng, K. K., et al. (2014). Magnetic resonance imaging (MRI) based finite element modeling for analyzing the influence of material properties on menisci responses. In Applied Mechanics and Materials (pp. 305–309). Trans Tech Publications.
28. I.N. Sneddon, The Relation between Load and Penetration in the Axisymmetric Boussinesq Problem for a Punch of Arbitrary Profile. Int. J. Eng. Sci.,1965, v. 3, pp. 47–57.
29. K.L. Johnson, Contact mechanics. Cambridge University Press, Ninth printing 2003.
30. Popov, V. L., Heß, M., Willert, E., Popov, V. L., Heß, M., & Willert, E. (2019). Normal Contact Without Adhesion. In Handbook of Contact Mechanics. https://doi.org/10.1007/978-3-662-58709-6_2
31. Halonen, K. S., et al. (2014). Deformation of articular cartilage during static loading of a knee joint–experimental and finite element analysis. Journal of Biomechanics, 47(10), 2467–2474.
32. Wang, Y., Fan, Y., & Zhang, M. (2014). Comparison of stress on knee cartilage during kneeling and standing using finite element models. Medical Engineering & Physics, 36(4), 439–447.
33. Hu, J., Chen, Z., Xin, H., Zhang, Q., & Jin, Z. (2018). Musculoskeletal multibody dynamics simulation of the contact mechanics and kinematics of a natural knee joint during a walking cycle. Proceedings of the Institution of Mechanical Engineers, Part H: Journal of Engineering in Medicine, 232(5), 508–519. https://doi.org/10.1177/0954411918767695
34. Lee, K. M., & Guo, J. (2010). Kinematic and dynamic analysis of an anatomically based knee joint. Journal of Biomechanics, 43(7), 1231–1236. https://doi.org/10.1016/j.jbiomech.2010.02.001
35. Duraisamy, Shriram., Gideon, Praveen, Kumar., Fangsen, Cui., Yee, Han, Dave, Lee., & Karuppasamy, Subburaj. (2017). Evaluating the effects of material properties of artificial meniscal implant in the human knee joint using finite element analysis. Scintific reports, 7:6011, DOI:10.1038/s41598-017-06271-3
36. Lee, E. H. (1955). Stress analysis in visco-elastic bodies. Quarterly of Applied Mathematics, 13(2), 183–190. https://doi.org/10.1090/qam/69741.
37. LD Landau, E.M. Lifschitz, Theory of elasticity (Theoretical Physics, Vol7), 3rd edition, 1999, Butterworth-Heinemann, Oxford, 8,9.
38. Radok, J. R. M. (1957). Visco-elastic stress analysis. Quarterly of Applied Mathematics, 15(2), 198–202. https://doi.org/10.1090/qam/92453
39. Fernandes, D. J. C. (2014). Finite element analysis of the ACL-deficient knee. Ph.D. thesis, IST, Universidade de Lisboa, Portugal.
40. Halonen, K.S., et al., deformation of articular cartilage during static loading of a knee joint – Experimental and finite element analysis. Journal of Biomechanics (2014), http://dx.doi.org/10.1016/j.jbiomech.2014.04.013
41. Chan, D., Cai, L., Butz, K. et al. In vivo articular cartilage deformation: non-invasive quantification of intratissue strain during joint contact in the human knee. Sci Rep 6, 19220 (2016). https://doi.org/10.1038/srep19220